Available online at www.sciencedirect.com

SciVerse ScienceDirect

Ceramics International 38 (2012) 6911–6917

CERAMICS INTERNATIONAL

www.elsevier.com/locate/ceramint

Short communication

Electron microscopy study of intragranular nanoporosity and the occurrence of local structural disorder in cubic $BaTiO_3$ nanopowders from alkoxide–hydroxide precipitation process

Tomasz M. Stawski[a], Sjoerd A. Veldhuis[a], Ole F. Göbel[a,1], Edyta Podstawka-Proniewicz[b], Johan E. ten Elshof[a,*]

[a] *MESA+ Institute for Nanotechnology, University of Twente, P.O. Box 217, 7500 AE Enschede, The Netherlands*
[b] *Regional Laboratory of Physicochemical Analysis and Structural Research of the Faculty of Chemistry, Jagiellonian University, Ingardena 3, 30-060 Kraków, Poland*

Received 16 April 2012; received in revised form 7 May 2012; accepted 7 May 2012
Available online 12 May 2012

Abstract

The evolution of phase and defect structure in $BaTiO_3$ nanopowders synthesized by an alkoxide–hydroxide process in benzyl alcohol under reflux conditions were investigated. As-prepared powders were heat-processed at temperatures ranging from 250 to 850 °C. X-ray powder diffraction (XRD) showed that $BaTiO_3$ remained cubic with crystallite size below 30 nm after heat treatment up to 850 °C. Internal pores of 1–2 nm diameter inside the crystallites were well visible with transmission electron microscopy (TEM) at processing temperatures between 250 and 600 °C. Their presence was confirmed by infrared spectroscopy (FT-IR) and is attributed to accumulation and curing of lattice hydroxyl defects. No tetragonal phase was detected by XRD up to 700 °C. However, Raman spectroscopy (FT-RS) revealed Raman activity in all cubic materials. This was attributed to local tetragonal and orthorhombic distortions, resulting from the presence of internal nanopores. Considering that the nanopores constitute a relatively large fraction of the total volume of the nanocrystals, the internal strain may be substantial. Hence, a relatively high temperature is necessary not only to cure the hydroxyl defects, but also to release the internal strains accumulated in the crystals upon volume diffusion and sintering. Therefore, the cubic-to-tetragonal phase transition was observed only after heat treatment at 850 °C, when the occurrence of a tetragonal phase was accompanied by substantial grain growth to ~100 nm size.
© 2012 Elsevier Ltd and Techna Group S.r.l. All rights reserved.

Keywords: B. Defects; B. Electron spectroscopy; B. Porosity; D. Barium titanate

1. Introduction

Barium titanate ($BaTiO_3$) is a high-*k* dielectric material used in commercial multi-layer ceramic capacitors. The minimum $BaTiO_3$ layer thickness that can be achieved with state of the art tape casting methods is about 1 μm, which implies the use of starting powders with a particle size of *ca.* 200 nm [1]. Further reduction of the barium titanate layer thickness requires finer powders obtained by new synthesis techniques. Barium titanate nanopowders can be synthesized by wet-chemical methods, yielding nanometer-sized particles (5–100 nm) of high purity and homogeneity, and of adjustable composition [2]. Among these methods the alkoxide–hydroxide sol precipitation route has received much attention [2–6]. It is a viable alternative to the alkoxide-carboxylate process, which requires high processing temperatures for the perovskite phase to crystallize [7]. The alkoxide–hydroxide sol precipitation route yields crystalline $BaTiO_3$ below 100 °C [3–6].

In the classical approach, titanium(IV) alkoxide is added dropwise to a basic aqueous solution of barium hydroxide with pH > 11, yielding highly agglomerated $BaTiO_3$ with crystal sizes > 100 nm. Precipitation in non-aqueous media has also been

*Correspponding author. Tel.: +31 53 489 2695; fax: +31 53 489 2990.
E-mail address: j.e.tenelshof@utwente.nl (J.E. ten Elshof).
[1] Present address: Bruker Nanoscience GmbH, Dynamostraße 19, 68165 Mannheim, Germany.

0272-8842/$36.00 © 2012 Elsevier Ltd and Techna Group S.r.l. All rights reserved.
http://dx.doi.org/10.1016/j.ceramint.2012.05.017

studied. A mixture of Ti(IV) isopropoxide and barium hydroxide in isopropanol precipitated directly into nanocrystalline (7.5 nm) barium titanate powder above 80 °C [8,9]. We studied an analogous reaction, and demonstrated that the reaction medium has a profound influence on the crystallinity and phase of the resulting product [10].

$BaTiO_3$ nanopowders with such small dimensions are known to exist predominantly in a non-ferroelectric cubic form instead of a tetragonal phase [1,11]. The highest dielectric response of $BaTiO_3$ is obtained at grain sizes of 700–1000 nm [1,11]. As the grain size decreases, the dielectric properties decrease and a cubic phase forms when the grain size is smaller than 200 nm. Such systems lack an observable tetragonal-to-cubic transition [12], and this has been explained in terms of (1) twinning of polycrystalline materials with decreasing grain size, (2) lack of driving force for the ferroelectric transition and depolarization fields, and (3) the defect structure of $BaTiO_3$ [11].

It is well known that wet-chemical processing yields hydroxyl defects in the barium titanate lattice structure at the positions of oxygen lattice sites. The resulting charged defects are probably compensated by vacancies in the cation sub-lattices, hence both by Ba and Ti vacancies [11,13,14]. It has been proposed that a high concentration of point defects interferes with the long-range polar ordering, which is the driving force for the cubic-to-tetragonal transition below the Curie temperature [11]. Hydroxyl defects have been observed in $BaTiO_3$ by infrared spectroscopy (FT-IR) [11,15] and Raman scattering [14]. In hydrothermal cubic powders with crystallite sizes above 200 nm, a temperature of 500 °C was sufficient to remove the majority of hydroxyl defects from the lattice [15]. Full restoration of tetragonality marked by reaching a unit cell parameter ratio $(c\text{-}a)/a = 1\%$ was observed at 600 °C [16], but in solvents like N-methy-2-pyrrolidinone [17] and dimethylformamide [18] the cubic-to-tetragonal transition can also occur without heat treatment. However, Begg et al. did not correlate water release with the occurrence of a tetragonal distortion at room temperature in hydrothermal barium titanate [19]. Frey and Payne suggested similarly that hydroxyl defect-containing barium titanate obtained by the alkoxide-carboxylate process did not undergo a cubic-to-tetragonal transition at room temperature due to defect curing, but due to grain growth from 35 to 100 nm [11]. Their conclusion was based on the observation that complete curing of hydroxyl defects took place only after heat treatment above 800 °C, while the cubic phase remained present until 1000 °C. Nonetheless, such hydroxyl defect-free nano-crystalline $BaTiO_3$ displayed Raman activity typical for orthorhombic and tetragonal phases when processed below 800 °C [11]. Similarly, Raman activity typical for the tetragonal phase was observed in particles as small as 17 nm without hydroxyl defects [20].

It thus seems that the "grain size" effect in $BaTiO_3$ is influenced by a number of factors like crystallite size, synthesis method, appearance (powder or sintered material) and reactivity upon heat processing [1]. The current work illustrates that two structural effects should actually be considered: (1) the occurrence of a tetragonal phase observable by X-ray diffraction (XRD) and Raman spectroscopy in barium titanate powders with crystallite sizes above a certain minimum value, and (2) the occurrence of local tetragonal/orthorhombic distortions, yielding Raman activity only. We demonstrate that the latter effect can be attributed to the presence of nanopores of 1–2 nm diameter inside crystals of sub-50 nm size.

2. Experimental

2.1. Materials

Titanium(IV) isopropoxide ($Ti[OCH(CH_3)_2]_4$, $>99.999\%$), and barium hydroxide octahydrate ($Ba(OH)_2 \cdot 8H_2O$, $>98\%$) were acquired from Sigma-Aldrich. Benzyl alcohol ($>99\%$) was purchased from Acros. The reactants were used as received from the suppliers without further purification and were stored in a water-free environment (<0.1 ppm H_2O). Benzyl alcohol was provided as water-free, and additionally dried by means of molecular sieves (molsieve 3 Å, Sigma-Aldrich).

2.2. Synthesis of $BaTiO_3$

A solution of 0.2 mol/dm^3 titanium(IV) isopropoxide in benzyl alcohol was prepared. Barium hydroxide octahydrate was added to this solution, so that the resulting molar ratio of Ba to Ti was 1.00. The mixture was stirred vigorously for 15 min to form a homogeneous precursor and then refluxed for 2 h at 175 °C under continuous stirring. The solution was dried on a watch glass at 60 °C for 72 h, forming a powder of nano-crystalline $BaTiO_3$ [10]. The powder was divided into several batches and heat-treated at temperatures between 250 and 700 °C for 24 h and at 850 °C for 8 h in air (heating and cooling rate 4 °C/min).

2.3. Characterization

X-ray powder diffraction patterns were measured on a diffractometer with a Cu anode and a Ni filter for Cu K_β radiation, $I_{K\alpha 2}:I_{K\alpha 1} = 1{:}2$ (Philips PW1830). Patterns were collected in a step-mode with a resolution of 0.01° and a counting time of 2.5 s/step. Angle-dependent instrumental broadening effects and diffraction pattern displacement were corrected for by means of a Si standard (the British Drug House) mixed with the powders. The diffraction data were further processed using the X'Pert HighScore Plus 2.1 software package. Peaks were fitted with *pseudo*-Voigt function profiles. The cell parameters were refined from the as-fitted profiles using the McMaille algorithm [21]. Crystallite sizes were obtained by the Scherrer algorithm

using full-width at half maximum (FWHM) data of several selected fitted profiles.

Powders heat-treated at various temperatures were dispersed in *iso*-propanol, sonicated for 10 min and deposited onto holey carbon copper grids (CF200-Cu, Electron Microscopy Sciences). Then the samples were dried at 60 °C for 1 h on a hot-stage and used for transmission electron microscopy (TEM) characterization (Philips CM300ST-FEG at 300 kV). Samples were investigated at low magnification to locate typical areas and features of interest were examined at high magnification.

Raman spectra (FT-RS) were recorded on a THERMO spectrometer (Nicolet 5700 NXR 9650) combined with a liquid nitrogen-cooled germanium detector. Typically between 300 and 4000 scans were collected with a resolution of 4 cm^{-1}. Excitation at 1064 nm from a continuum-wave Nd^{3+}:YAG laser was used. The output power was set to 100 mW. No thermal degradation of the sample was observed during the measurements.

Infrared spectra (FT-IR) were recorded in an attenuated-total-reflection mode (ATR) (Bruker Tensor 27 equipped with DLaTGS detector, and Pike GladiATR). Typically between 128 and 256 scans were collected with a resolution of 4 cm^{-1}.

3. Results and discussion

3.1. Powder diffraction

X-ray diffraction patterns of as-synthesized powders and powders heat-treated between 250 and 850 °C are presented in Fig. 1A. All diffraction patterns were attributed to $BaTiO_3$. Traces of impurities were attributed to barium carbonate. The FWHM of the diffraction peaks decreased with increasing calcination temperature, and a temperature-dependent shift of diffraction peaks to higher 2θ was noticeable (see peak around 2θ 39.0° in inset of Fig. 1A), indicating crystallite growth and shrinkage of the unit cell, respectively. A characteristic splitting of some peaks, indicative of a tetragonal distortion, occurred in the powder calcined at 850 °C (peak around 2θ 45.0°, see inset in Fig. 1A). All patterns were fitted with *pseudo*-Voigt peak profiles. This provided information on peak positions and full width at half maximum (FWHM), corrected for instrumental broadening effects. An example fit to the pattern of the powder heat-treated at 850 °C is given in Fig. 1B.

The crystallite size as a function of calcination temperature based on Scherrer analysis is shown in Fig. 1C. The unit-cell parameters were obtained and refined using the McMaille algorithm assuming space group *Pm-3m* for samples up to 700 °C, and *P4mm* for the powder processed at 850 °C (Fig. 1D). The as-synthesized powder and a powder that was heat-treated at 250 °C for 24 h had an average crystallite size of 10 ± 2 nm. Heat-treatment at 850 °C led to a substantial grain growth up to 50 ± 15 nm after calcination for 8 h. No clear indications for the presence of a tetragonal phase was found by XRD below 850 °C. Nevertheless, the unit cell volume V and lattice constants decreased gradually with increasing temperature (Fig. 1D). For the as-synthesized powder, $a = 4.0345(2)$ Å and $V = 65.6715(4)$ $Å^3$. After processing at 850 °C, a tetragonal phase with $V = 64.1919(8)$ $Å^3$ and $(c-a)/a = 0.78\%$ was observed.

3.2. TEM imaging

Fig. 2A shows the typical morphology of as-synthesized powders and of material calcined at 250 °C for 24 h. Highly crystalline nanoparticles with sizes below 10 nm were predominant. Spherical defects with lower electron density can be recognized within some of the grains, and these are marked by a broken circle. The concentration of such defects in powders treated at higher temperature was considerably higher than the number of defects in the as-synthesized material. The internal nano-porosity probably developed as a result of accumulation of hydroxyl defects through diffusion at elevated temperatures, followed by H_2O formation and evaporation. Thermal processing at 350 − 450 °C yielded barium titanate with comparable microstructures. The presence of spherical internal defects became more pronounced at 400 °C and higher (Fig. 2B).

Processing at 500 °C changed the microstructure of $BaTiO_3$ powders significantly, as shown in Fig. 3A. Intragranular nanoporosity was still present, and neither the shape nor the size of the pores changed considerably. Inset II in Fig. 3A shows a typical grain with internal pores. Further temperature increase to 600 °C did not affect crystallite size, morphology or porosity, but internal porosity was absent in powders processed at 650 (Fig. 3B) and 700 °C.

3.3. Vibrational FT-RS and ATR-IR characterization

Raman scattering spectra of $BaTiO_3$ are shown in Fig. 4A. Apart from the peak around 690 cm^{-1}, which was attributed to a carbonate impurity, the Raman activity demonstrates the presence of an asymmetric local structure in $BaTiO_3$ [14,22–24]. Although cubic barium titanate does not exhibit Raman activity, broad Raman bands at 520 and 250 cm^{-1} have been observed in cubic barium titanate [23,24]. They were attributed to local disorder of Ti ions in an overall cubic lattice.

In tetragonal $BaTiO_3$ with *P4mm* symmetry one would expect a peak with a centroid around 260 cm^{-1}—A_1(TO) optical mode; a sharp peak at 315 cm^{-1}—B_1, E(TO + LO) optical mode; an asymmetric broad peak at 520 cm^{-1}—A_1, E(TO) optical mode; and a broad peak at around 720 cm^{-1}—A_1, E(LO) [24]. All these peaks were actually present in the samples processed at 850 °C, where $BaTiO_3$ was tetragonal according to XRD. The dip around 180 cm^{-1} in the same sample has been attributed to anharmonic coupling between three A_1(TO) phonons [23,24]. However, in all powders calcined at $T < 850$ °C,

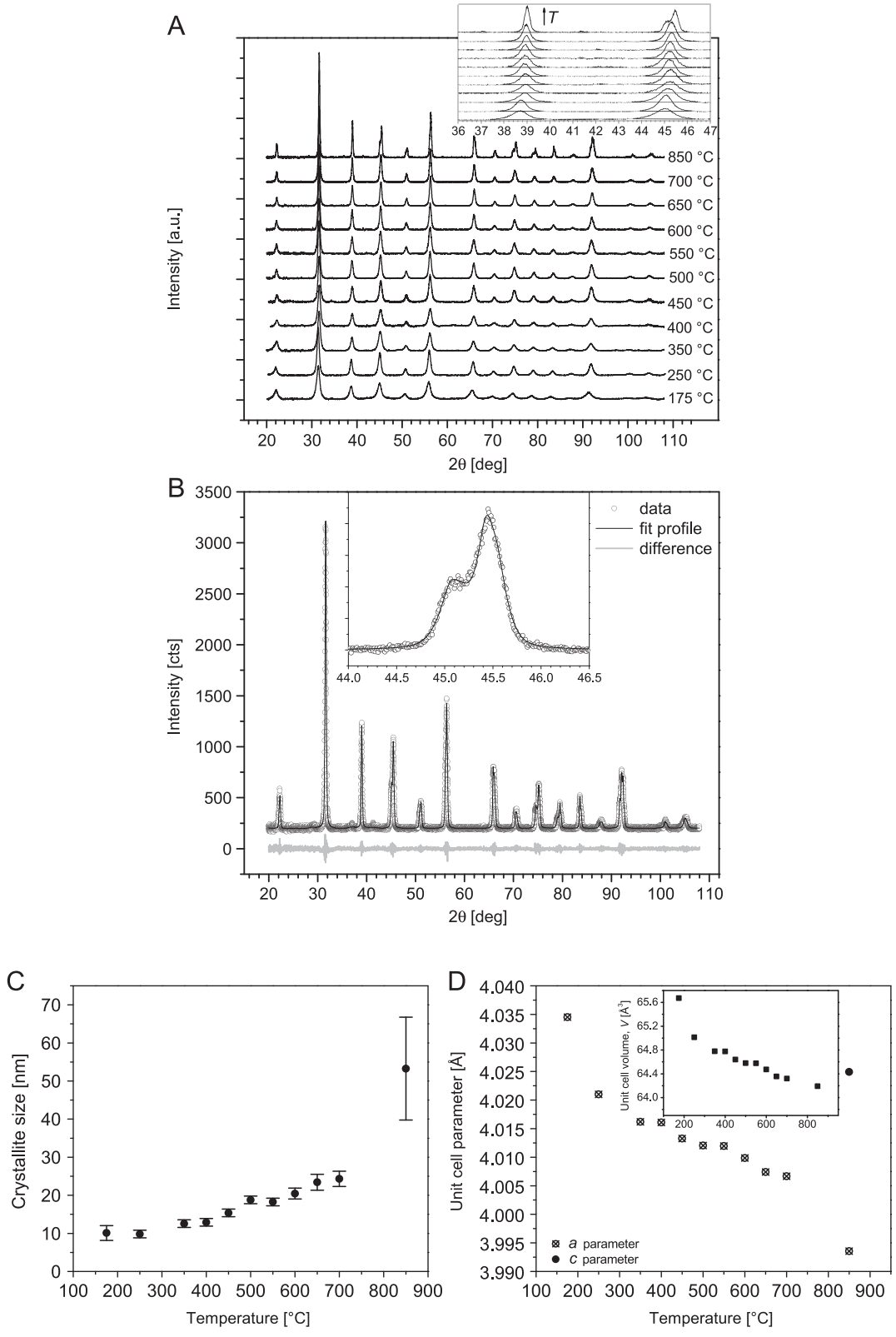

Fig. 1. (A) XRD patterns of as-synthesized and heat-treated $BaTiO_3$ powders. Inset shows shift and splitting of selected diffraction peaks to higher angles with increasing calcination temperature; (B) Example fit of pseudo-Voigt function profile to XRD pattern of powder heat-treated at 850 °C. Inset shows split (002)/(200) peaks of tetragonal $BaTiO_3$; (C) Average crystallite size as function of processing temperature. (D) Unit cell parameters as function of processing temperature. Inset shows unit cell volume with temperature.

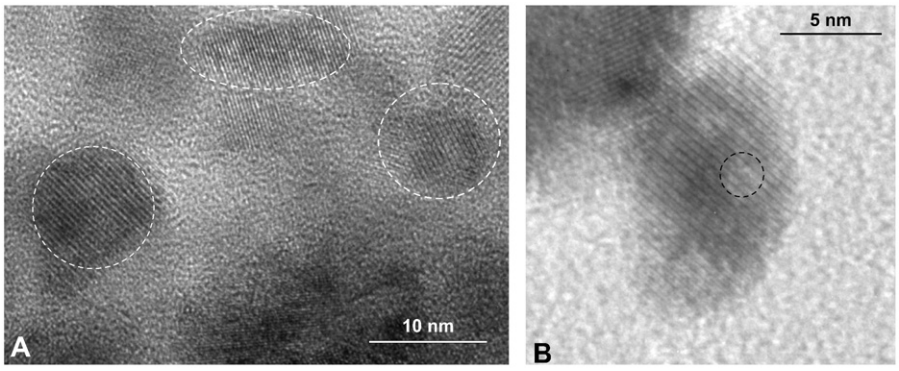

Fig. 2. Bright-field HR-TEM images of $BaTiO_3$ powders: (A) heat-treated at 250 °C for 24 h and (B) Crystallite after heat treatment at 400 °C. Examples of crystals with internal pore-like defects are marked with broken circles.

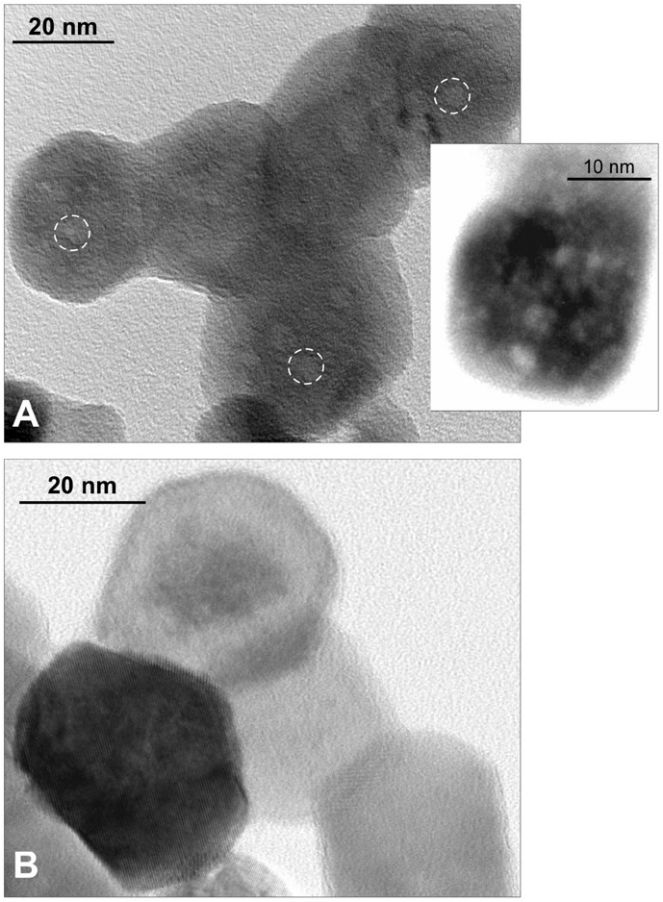

Fig. 3. Bright-field HR-TEM image of $BaTiO_3$ powder: (A) $T=500$ °C for 24 h. Inset shows a crystallite with a focal plane selected to emphasize the internal nanoporosity; (B) $T=650$ °C for 24 h.

which were cubic according to XRD, the same feature took the form of a peak at 190 cm^{-1}. It is thought to result from phonon damping caused by internal stress, defects, or the presence of an orthorhombic phase [11,23,24].

The peak at 308 cm^{-1} can be attributed to the B_1, $E(TO+LO)$ phonon mode. It suggests the presence of (local) tetragonal symmetry in samples processed above 250 °C. The same peak was virtually absent in the as-synthesized powder. Peaks at 717 cm^{-1} and 519 cm^{-1} behaved similarly. No peaks were found in the proximity of 810 cm^{-1}. These would have indicated the presence of internal hydroxyl lattice defects [23]. On the other hand, the presence of hydroxyl defects in the lattice and/or OH groups at the surface was confirmed by ATR-IR spectra in the range between 4000 cm^{-1} and 2500 cm^{-1} (Fig. 4B), where a broad band originating from surface adsorbed water or alcohol (*e.g.* benzyl alcohol) was present. A weak peak/shoulder at 3550 cm^{-1} was noticeable in powders calcined up to 600 °C, which can be attributed to lattice hydroxyl defects [13–15]. These lattice hydroxyls disappeared above 600 °C, in agreement with the disappearance of internal nanopores from the TEM images at the same temperatures.

3.4. Data interpretation

A consistent image of the phase evolution of alkoxide–hydroxide-precipitated nanosized $BaTiO_3$ emerged from the experimental data. As-synthesized barium titanate was cubic in XRD and FR-RS, with average crystallite sizes <10 nm. The large unit cell volume at this stage can be attributed to the presence of OH^- or/and CO_3^{2-} defects in the perovskite lattice [11,15]. The decrease of unit cell size with increasing processing temperature can be rationalized in terms of hydroxyl defect curing, which is known to occur at temperatures from 100 to 800 °C [11,15,25]. TEM analysis of as-synthesized and heat-treated nanopowders revealed the presence of internal nanoscale porosity. Probably these pore defects became only visible after diffusional accumulation of hydroxyl defects, followed by their annihilation via H_2O formation.

Hennings et al. reported internal porosity in hydrothermal powders after heat treatment above 500 °C. The loss of porosity was associated with hydroxyl defect migration and annihilation according to the model proposed by Hennings et al. [14,25]. However, the intragranular pores in that study had dimensions from a few to 200 nm. In our study we observed pores with a size of only few nanometers far below 500 °C. The difference may be related to

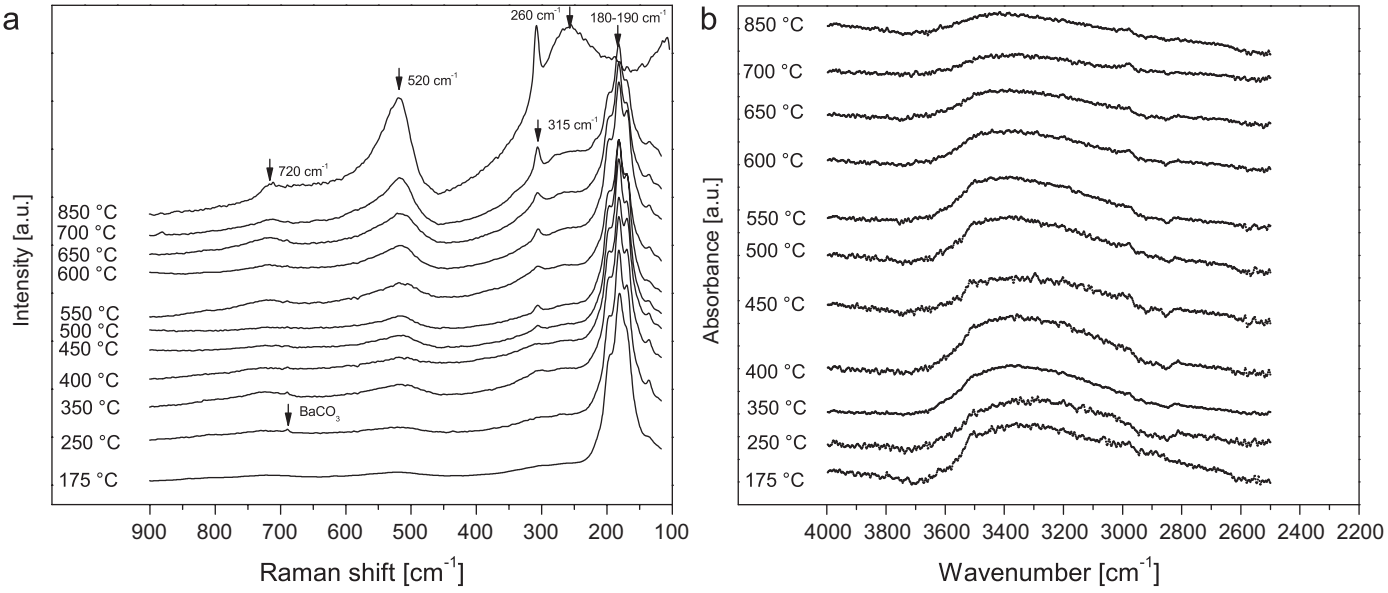

Fig. 4. (a) FT-RS spectra of as-synthesized and heat-treated $BaTiO_3$ powders. $BaCO_3$ phase is marked; (b) ATR-IR spectra of as-synthesized and heat-treated $BaTiO_3$ powders in the wavelength region typical for hydroxyl defects.

the higher reactivity of sub-10 nm powders compared to the hydrothermal crystallites of 200 nm size in the study of Hennings et al. TEM and XRD of powders heat-treated at 650 and 700 °C showed significant shrinkage of the unit cell. But no more internal porosity was observed at these temperatures with TEM, and ATR-IR also indicated the absence of internal hydroxyls.

Raman activity was detected in all powders after processing up to 700 °C, with clear signals at 190, 308 and 519 cm^{-1}. Since these materials are cubic according to XRD, the Raman peaks indicates the occurrence of significant local deviations from cubic symmetry in the crystallites. Local structural disorder is visible by spectroscopic methods, but not by XRD. In the present case the disorder is most likely caused by internal point defects and/or lattice strain by internal pores. The presence of a peak at 308 cm^{-1} suggests local tetragonal symmetry, while the positive peak in the Raman spectra around 190 cm^{-1} can be attributed to local orthorhombic symmetry or internal stress. The latter peak was also observed by Frey and Payne in sol–gel derived powders [11]. The minimum at 180 cm^{-1} coincides with crystallographic tetragonality in XRD, suggesting that these two observations are correlated.

Stabilization of the cubic phase at room temperature is often attributed to the excessive surface energy or high hydrostatic pressure in $BaTiO_3$ nano-powders, which can be lowered via grain growth upon annealing [11,19,26,27]. This theory explains the observed cubic-to-tetragonal transition after annealing at 850 °C, but it does not explain the Raman activity of powders that were heat-treated at considerably lower temperatures when only limited grain growth had taken place. We hypothesize that removal of hydroxyl defects from as-synthesized powders upon heating leads to pore formation, which results in local strains inside particles and to local non-correlated distortions around Ti^{4+} ions. This results in Raman activity that can be attributed to local tetragonal or orthorhombic symmetry. Considering that these nanopores constitute a relatively large fraction of the total volume of a nanocrystal, the internal strains may be substantial. Hence, a relatively high temperature is necessary not only to cure the hydroxyl defects, but also to release the internal strains accumulated in the crystals upon volume diffusion and sintering.

4. Conclusions

The phase evolution of the $BaTiO_3$ nanocrystalline powder can be explained in terms of two effects:

(1) As-synthesized sub-10 nm $BaTiO_3$ nanocrystals contained internal nanopores after processing at all temperatures below 500 °C. The Raman activity in these materials can be attributed to a local tetragonal or orthorhombic distortion of the cubic lattice. The internal hydroxyl groups and intragranular nanoporosity disappeared only at 600 °C.
(2) The high-temperature treatment at 600 °C required to fully remove the hydroxyl defects was accompanied by substantial grain growth. Tetragonal particles of ~100 nm diameter evolved from cubic sub-25 nm crystallites. This finally resulted in the formation of a fully tetragonal $BaTiO_3$ phase at 850 °C.

Acknowledgments

Financial support by the Netherlands Technology Foundation STW is gratefully acknowledged.

References

[1] D. Yoon, Tetragonality of barium titanate powder for a ceramic capacitor application, Journal of Ceramic Processing Research 7 (2006) 343–354.

[2] C. Pithan, D.H. Hennings, R. Waser, Progress in the synthesis of nanocrystalline $BaTiO_3$ powders for MLCC, International Journal of Applied Ceramic Technology 2 (2005) 1–14.

[3] S.S. Flaschen, An Aqueous Synthesis of Barium Titanate, Journal of the American Chemical Society **77** (1955) 6194.

[4] F. Chaput, J.P. Boilot, Chemical processing of $(Ba,Sr)(Ti,Zr)O_3$ perovskite ceramics, Journal of Materials Science Letter 6 (1987) 1110–1112.

[5] F. Chaput, J.P. Boilot, A. Beauger, Alkoxide-hydroxide route to synthesize $BaTiO_3$ based powders, Journal of the American Ceramic Society 73 (1990) 942–948.

[6] N.V. Golubko, M.I. Yanovskaya, I.P. Romm, Preparation of barium titanate and related materials by the alkoxide-hydroxide route, Journal of Sol-Gel Science and Technology 20 (2001) 135–143.

[7] M.H. Frey, D.A. Payne, Synthesis and processing of barium titanate ceramics from alkoxide solutions and monolithic gels, Chemistry of Materials: A Publication of the American Chemical Society 7 (1995) 123–129.

[8] S. Yoon, S. Baik, M.G. Kim, N. Shin, Formation mechanisms of tetragonal barium titanate nanoparticles in alkoxide-hydroxide sol-precipitation synthesis, Journal of the American Ceramic Society 89 (2006) 1816–1821.

[9] S. Yoon, S. Baik, M.G. Kim, N. Shin, I. Kim, Synthesis of tetragonal barium titanate nanoparticles via alkoxide-hydroxide sol-precipitation: effect of water addition, Journal of the American Ceramic Society 90 (2007) 311–314.

[10] T.M. Stawski, S.A. Veldhuis, O.F. Göbel, J.E. Ten Elshof, D.H.A. Blank, Effects of reaction medium on the phase synthesis and particle size evolution of $BaTiO_3$, Journal of the American Ceramic Society 93 (2010) 3443–3448.

[11] M.H. Frey, D.A. Payne, Grain-size effect on structure and phase transformations for barium titanate, Physical Review B 54 (1996) 3158–3168.

[12] M. Yashima, T. Hoshina, D. Ishimura, S. Kobayashi, W. Nakamura, T. Tsurumi, S. Wada, Size effect on the crystal structure of barium titanate nanoparticles, Journal of Applied Physics 98 (2005) 014313-1–014313-8.

[13] I. Laulicht, L. Benguigui, Infrared spectra of hydrogen impurities in $BaTiO_3$ crystals, Solid State Communications 32 (1979) 771–775.

[14] T. Noma, S. Wada, M. Yano, T. Suzuki, Analysis of lattice vibration in fine particles of barium titanate single crystal including the lattice hydroxyl group, Journal of Applied Physics 80 (1996) 5223–5233.

[15] D. Hennings, S. Schreinemacher, Characterization of hydrothermal barium titanate, Journal of the European Ceramic Society 9 (1992) 41–46.

[16] Y.-I. Kim, J.K. Jung, K.-S. Ryu, Structural study of nano $BaTiO_3$ powder by Rietveld refinement, Materials Research Bulletin 39 (2004) 1045–1053.

[17] R. Kota, B.I. Lee, Effect of lattice hydroxyl on the phase transition and dielectric properties of barium titanate particles, Journal of Materials Science: Materials in Electronics 18 (2007) 1221–1227.

[18] P. Badheka, L. Qi, B.I. Lee, Phase transition in barium titanate nanocrystals by chemical treatment, Journal of the European Ceramic Society 26 (2005) 1393–1400.

[19] B.D. Begg, E.R. Vance, J. Nowotny, Effect of particle size on the room-temperature crystal structure of barium titanate, Journal of the American Ceramic Society 77 (1994) 3186–3192.

[20] S. Wada, H. Yasuno, T. Hoshina, S.-M. Nam, H. Kakemoto, T. Tsurumi, Preparation of nm-Sized barium titanate fine particles and their powder dielectric properties, Japanese Journal of Applied Physics 42 (2003) 6188–6193.

[21] A. Le Bail, Monte Carlo indexing with McMaille, Powder Diffraction 19 (2004) 249–254.

[22] B.D. Begg, K.S. Finnie, E.R. Vance, Raman study of the relationship between room-temperature tetragonality and the curie point of barium titanate, Journal of the American Ceramic Society 79 (1996) 2666–2672.

[23] Y. Shiratori, C. Pithan, J. Dornseiffer, R. Waser, Raman scattering studies on nanocrystalline $BaTiO_3$ Part I – isolated particles and aggregates, Journal of Raman Spectroscopy 38 (2007) 1288–1299.

[24] U.D. Venkateswaran, V.M. Naik, R. Vaik, High-pressure raman studies of polycrystalline $BaTiO_3$, Physical Review B 58 (1998) 14256–14260.

[25] D.F.K. Hennings, C. Metzmacher, B.S. Schreinemacher, Defect chemistry and microstructure of hydrothermal barium titanate, Journal of the American Ceramic Society 81 (2001) 179–182.

[26] K. Uchino, E. Sadanaga, T. Hirose, Dependence of the crystal structure on particle size in barium titanate, Journal of the American Ceramic Society 72 (1989) 1555–1558.

[27] F. Yen, C.T. Chang, Y. Chang, Characterization of barium titanyl oxalate tetrahydrate, Journal of the American Ceramic Society 73 (1970) 3422–3427.